Quantum calculations of At-mediated halogen bonds: on the influence of relativistic effects

Nicolas Galland, Gilles F Montavon, Jean-Yves Le Questel, Jérôme Graton

Quantum calculations of At-mediated halogen bonds: on the influence of relativistic effects

N. Galland[a], G. Montavon[b], J.-Y. Le Questel[a] and J. Graton[a]

The infuence of relativistic effects, more specifically of spin–orbit coupling (SOC), on the geometric and energetic features of halogen bonds mediated through astatine (At) has been investigated through quantum chemistry calculations. For complexes between ammonia and diastatine or diiodine, the accounting of SOC results in stronger interaction energies with iodine, in contrast to scalar-relativistic calculations which predict astatine as a better halogen-bond (XB) donor. In AtI, where the competition is intramolecular, astatine always appears as the strongest XB donor. Whereas calculations in the absence of SOC predict that 15% of the XB complexes with toluene occur on the iodine atom, this population becomes three times lower when SOC is taken into account. The investigation of hypoastatous acid properties highlights a substantial decrease of the hydrogen-bond (HB) and XB interaction energies for AtOH when SOC is considered. The calculation of complementary electrostatic (electrostatic potential, $V_{S,max}$) and charge transfer (local electrophilicity, $\omega^{+}_{S,max}$) descriptors provide guidelines for the rationalization of these trends, underlining the significant role of SOC in astatine electronegativity. Finally, the SOC effects are shown in AtI and AtOH to be significantly transferred from astatine to its neighbouring atoms, resulting in stronger alterations of their XB or HB properties than on the XB donating ability of astatine itself.

Introduction

Astatine (At, $Z = 85$) is a radioelement, which takes its name from the greek ''astatos'' (unstable) because it has no stable isotopes. Its longest-lived isotope, ^{210}At, has a half-life of 8.1 hours. Astatine is thus the rarest element naturally occurring on Earth (its total amount present at any given time is estimated between a few hundred milligrams and 30 g).[1,2] The second ''long''-lived isotope, ^{211}At, exhibits a half-life time of 7.2 h and a yield of 100% of α-particle emission, two favourable physical properties for applications in nuclear medicine. Hence, it is one of the most promising radionuclides for systemically targeted alpha therapy of cancers.[3–5] Outside the biomedical context,[6–8] astatine also exhibits chemical properties similar to its neighbour iodine,[9,10] and to other halogens,[11,12] which establish this radioelement as the heaviest element in the halogen family to date. Owing to its higher polarizability in comparison with iodine,[13] At is expected to be the strongest halogen-bond donor.[14] Unfortunately, little is known at this time about the ability of astatine species to form halogen bonds (XBs) because of the impossibility to use conventional spectroscopic tools to characterize astatinated species. Indeed, one can only work at ultra-trace concentrations (typically below 10^{-10} mol L^{-1}) because of the very small amounts of produced At atoms,[2] critically limiting the useful experimental techniques. However, some of us recently overcame this challenge and reported the first experimental evidence of halogen bond interactions involving astatine.[15] Complexation constants of astatine monoiodide (AtI) with a series of Lewis bases were derived from distribution coefficient measurements in an aqueous/cyclohexane biphasic system. AtI appeared as a stronger halogen-bond donor than diodine (I_2), and further relativistic quantum mechanical calculations supported the claim that the XB interactions are really mediated by astatine. Theoretical calculations indeed appeared as useful tools to investigate the chemistry of astatine at the molecular level,[16–24] and, for the reason given above, the former articles dealing with the XB donating ability of astatine were pure theoretical investigations. Alkorta *et al.* first studied the competition between hydrogen bonds and halogen bonds in complexes of hypohalous acids HOX (X = F, Cl, Br, I, and At) with nitrogenated bases.[25] This competition was also investigated for astatinated 1-methyluracil in recent works of van Mourik and co-workers.[26,27] On their side, Hill and Hu established benchmark XB geometries and interaction energies on prototypical systems, that is XY dihalogens (X, Y = F, Cl, Br, I, and At) bound to ammonia.[28] The results of these studies support the assumption that astatine is a stronger XB donor than iodine is, making astatine the strongest halogen-bond donor.

[a] *Laboratoire CEISAM, UMR CNRS 6230, Université de Nantes, 2 rue de la Houssinière, BP 92208, Nantes Cedex 3, 44322, France. E-mail: Nicolas.Galland@univ-nantes.fr, Jerome.Graton@univ-nantes.fr*

[b] *Laboratoire SUBATECH, UMR CNRS 6457, IN2P3/EMN Nantes/Université de Nantes, 4 Rue Alfred Kastler, BP 20722, Nantes Cedex 3, 44307, France*

However, most of the published theoretical works actually lack a proper description of an important effect inherent to At, namely the spin–orbit coupling (SOC). As a heavy element, the properties of astatine and of its compounds can be strongly affected by the relativistic effects. The latter are traditionally split in two types of terms, the ''scalar'' and ''spin-dependent'' ones. The main spin-dependent effect, which results from the interaction of the electron spin with magnetic fields generated by charges in relative motion, is the spin–orbit coupling. The SOC effects can be of similar magnitude than the scalar-relativistic effects for heavy p-elements. While scalar-relativistic calculations can routinely be performed using most quantum chemistry codes, the treatment of the spin–orbit interaction is less common. However, numerous studies have demonstrated the important effects of SOC on physicochemical properties of astatine-containing species (see for instance ref. 13, 17 and 29–35). We propose to review some of the few published articles to date on the properties of At-mediated halogen bonds, and to extract from each of them one significant feature revealing how neglecting SOC in calculations may lead to erroneous (or not complete) conclusions.

Computational methodology

Several efficient theoretical approaches to treat relativistic effects were developed in the recent years.[36–39] For studying compounds of a few tens of atoms, there is an interest in using DFT based approaches. We have selected the two-component (2c) relativistic density functional theory (DFT) approach that was proved to be reliable for the characterization of a wide range of At-compounds.[17,30,32,40–42] The spin–orbit DFT (SODFT) method available in the NWChem program package[43] makes use of pseudo-potentials (PPs) which contain scalar and spin-dependent potentials. Therefore, electron correlation and relativistic effects, including the spin–orbit coupling, are treated on an equal footing in the variational treatment. The hybrid meta PW6B95 exchange–correlation functional[44] was selected as (i) it was especially developed to be accurate for thermochemistry and non-covalent interactions, including XBs, and (ii) it appeared as the overall best choice among 36 DFT functionals recently tested on At-compounds.[35] The ECP*n*MDF small-core PPs were used to mimic the role of n = 10, 28 and 60 core electrons of Br, I and At atoms, respectively.[45,46] Their remaining 25 electrons were dealt with the correlation consistent aug-cc-pVTZ-PP basis sets,[45,46] supplemented for the I and At atoms by the 2c extensions described in ref. 47. For all the other atoms, the triple-zeta quality aug-cc-pVTZ basis sets were used[48–50] and abbreviated as AVTZ in the following. The energies of the XB complexes were corrected from the basis set superposition error (BSSE) using the counterpoise method.[51] In order to evaluate SOC effects on the studied species, geometry optimizations and frequency calculations have also been carried out at the scalar-relativistic DFT level of theory, *i.e.* in the absence of spin-dependent potentials in ECP*n*MDF PPs.

In order to assess the reliability of the PW6B95/AVTZ calculations, some coupled cluster CCSD(T) calculations were performed in conjunction with quadruple-zeta versions of the above basis sets (referred to as AVQZ throughout the text). The single point CCSD(T)/AVQZ calculations were performed on top of the previously optimized PW6B95/AVTZ geometries, using the frozen-core approximation (*e.g.* the 5s5p5d electrons of At were kept frozen as well as the 1s electrons of O in the AtOH species), and at a scalar-relativistic level of theory for species involving heavy atoms. Furthermore, the calculations of equilibrium constants in cyclohexane solution required to compute the solvation free energies of XY and XY$\cdots$toluene species (X, Y = At, I). We used the implicit solvation model recommended in a recent benchmark study focused on At-compounds,[35] which combines the UAHF cavities with the C-PCM continuum model[52] available in the Gaussian program package.[53] Note that we have used for At a basic radius of 2.41 Å[16] and, according to the original formulation of the UAHF cavity model,[54] the electrostatic scaling factor used to multiply the sphere radii was 1.2. Energy calculations were performed at the 2c-HF/AVTZ level of theory on top of the previously optimized 2c-PW6B95/AVTZ geometries. Regarding the calculations of local electrophilicity values, we used the finite difference method within the framework of conceptual density functional theory. More precisely, the electronegativity, $\chi = \frac{1}{2}(\mathrm{IP} + \mathrm{EA})$, and the hardness, $\eta = (\mathrm{IP} - \mathrm{EA})$, are computed from the vertical ionization potential (IP) and electron affinity (EA) values. Furthermore, the Fukui function for nucleophilic attack, $f^{+}(r)$, is obtained as:

$$f^{+}(r) \approx \rho_{N+1}(r) - \rho_{N}(r)$$

where ρ_N and ρ_{N+1} represent the electron density of the neutral species (N electrons) and of the corresponding anion (N + 1 electrons) at fixed geometry, respectively. The electron densities and the electrostatic potential values were computed using the Turbomole program package.[55]

Results and discussion

Diastatine *vs.* diiodine halogen-bond interactions

In a computational investigation, Hill and Hu provided benchmark quality geometries and interaction energies of the halogen-bond complexes of ammonia with the exhaustive series of dihalogen XY structures.[28] Based on their results at the CP-CCSD(T)-F12b/VTZ-F12 level of theory, they concluded that ''an increase in polarisability of the dihalogen produces an increase in interaction energy'', and ''this trend also applies to the astatine containing molecules''. Hence, one might anticipate that the strength of the halogen bonds increases downward along the halogen family. Focusing on calculations for the I_2 and At_2 dihalogen systems, we will show that this assumption breaks down when appropriate levels of theory are selected.

Our results on the $X_2\cdots NH_3$ (X = I, At) complexes are gathered in Table 1, the reference spin–orbit free data from Hill and Hu being also given for comparison. The results from the PW6B95/AVTZ calculations, in the absence of SOC, are found in excellent agreement with the CP-CCSD(T)-F12b/VTZ-F12 values. For instance, the average deviation on the computed

Table 1 Optimized intermolecular and intrahalogen bond lengths (in Å), variation of the intrahalogen bond length (in Å) as a result of $X_2\cdots NH_3$ formation, and counterpoise corrected interaction energy (in kcal mol^{-1})

	$d_{X\cdots N}$	d_{X-X}	Δd_{X-X}	ΔE^{CP}
$I-I\cdots NH_3$				
CP-CCSD(T)-F12b/VTZ-F12[28]	2.767	2.720	+0.041	−7.90[a]
PW6B95/AVTZ	2.721	2.725	+0.056	−8.22
2c-PW6B95/AVTZ	2.729	2.740	+0.053	−8.02
ΔSO[b]	+0.008	+0.015	−0.003	+0.20
$At-At\cdots NH_3$				
CP-CCSD(T)-F12b/VTZ-F12[28]	2.782	2.900	+0.042	−9.54[a]
PW6B95/AVTZ	2.754	2.899	+0.055	−9.68
2c-PW6B95/AVTZ	2.849	3.017	+0.022	−7.53
ΔSO[b]	+0.095	+0.118	−0.033	+2.15

[a] Extrapolation to the complete basis set limit. [b] The spin–orbit coupling effect (ΔSO) is defined as the difference between two-component relativistic and scalar-relativistic PW6B95/AVTZ values.

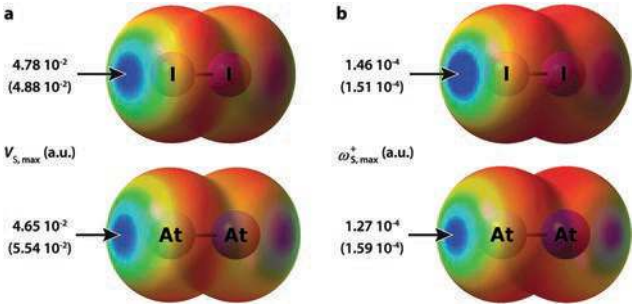

Fig. 1 2c-PW6B95/AVTZ calculated electrostatic potential (a) and local electrophilicity (b) at the At_2 and I_2 molecular surfaces (defined by 0.001 a.u. isovalues of the electron density). Values of $V_{S,max}$ and $\omega^+_{S,max}$ given in parentheses, come from spin–orbit free PW6B95/AVTZ calculations. Colour code: from red (lowest values) to blue (highest values).

intermolecular bond length is of 1.3%, and amounts to 2.8% for the interaction energy (the energy difference between the XB complex and the sum of the isolated monomers in their minimum energy configuration). Note that, when the geometry optimization is counterpoise corrected according to the strategy that was used in ref. 28, the geometrical parameters are even found in better agreement with the reference spin–orbit free values (Table S1 in ESI†). Thus, the selected DFT functional and basis sets appear well suited for studying $I_2\cdots NH_3$ and $At_2\cdots NH_3$. According to these results, one could conclude erroneously that the strength of the halogen bond in the $X_2\cdots NH_3$ series increases downward along the halogen family. The SOC relativistic effect is known to weaken the bonds involving astatine, and to a lesser extent those involving iodine, in many systems.[13,17,30–35,56–59] Here, the SOC effect (ΔSO) is defined as the difference between the results of two-component relativistic and scalar-relativistic PW6B95/AVTZ calculations. For instance, the intermolecular bond length in $At_2\cdots NH_3$ is increased by 3.4% while the interaction energy is reduced by 22.2%. Note that the properties of the $I_2\cdots NH_3$ complex are much less (approximately one order of magnitude) affected by the SOC. As a consequence, the complex of ammonia with diiodine is calculated to be 0.5 kcal mol^{-1} stronger than with diastatine at the 2c-PW6B95/AVTZ level of theory. This result is in clear contrast with the spin–orbit free calculations where the $At_2\cdots NH_3$ complex is favoured by 1.5–1.6 kcal mol^{-1}, and with the assumption that the halogen-bond interactions would be stronger for the heaviest (and more polarizable) halogen atoms.

Actually, intrinsic properties of the I_2 and At_2 monomers corroborate this result. A positive value of the electrostatic potential at the molecular surface (MEP), when observed along the axis of the chemical bond to the halogen atom, is usually referred as the "σ-hole".[60] This region can interact favourably with electron rich sites, thus giving rise to halogen bonding. The local maximum value of the MEP, $V_{S,max}$, is a descriptor commonly used to characterize the donating ability of a given XB donor.[14,61] The characteristics of these σ-holes are displayed for the At_2 and I_2 species on Fig. 1a. Beyond the recognized electrostatic origin of halogen bonding, it is now well established that the charge-transfer interaction also plays a significant role in the XB stabilization, especially for strong XBs.[14,28,61,62] Therefore, a more complete picture of the XB donating ability can be obtained from a second descriptor related to orbital-controlled (charge transfer) interactions[63] in addition to charge-controlled ones ($V_{S,max}$). To this end, we have selected from conceptual density functional theory, the local philicity $\omega(r)$ that was proven to be appropriate to quantify orbital-controlled reactivity.[64] This descriptor is defined as the product between the global electrophilicity index ω ($\chi^2/2\eta$) of the system and the so-called Fukui function, $f(r)$. For the characterization of the XB donor, which is prone to accept electrons, one must consider the $f^+(r)$ Fukui function, which gives rise to the local electrophilicity $\omega^+(r)$. It is shown on Fig. 1b that the computed values of the local electrophilicity at the molecular surfaces of At_2 and I_2 clearly highlight the structure of the σ-hole for both species. Located on the outer side of the halogen atom, the most positive electrophilicity value $\omega^+_{S,max}$ can be viewed as the complementary analogue of the $V_{S,max}$ descriptor, dedicated to probe the charge transfer component of the XB stabilization. At the PW6B95/AVTZ level of theory, *i.e.* in the absence of SOC, both $V_{S,max}$ and $\omega^+_{S,max}$ values are found larger for At_2 than for I_2 (Fig. 1). Hence, the At_2 species appears as the strongest XB donor when solely scalar-relativistic effects are accounted for. While the SOC hardly affects the $V_{S,max}$ and $\omega^+_{S,max}$ values in the case of the I_2 species, these descriptors in At_2 are decreased by 16.1% and 20.4%, respectively. As a consequence, the values of $V_{S,max}$ and $\omega^+_{S,max}$ are larger for I_2 at our most accurate level of theory, namely 2c-PW6B95/AVTZ, revealing *in fine* a better donating ability than At_2. These results corroborate the stronger interaction energies highlighted for the $I_2\cdots NH_3$ complex when SOC is taken into account.

Astatinated *vs.* iodinated halogen-bond interactions in AtI

In the previous paragraph, iodine is revealed to be a competitive XB donor towards astatine, at least when the comparison is done between the homonuclear diatomic systems. This competition is expected to reach its utmost in astatine monoiodide, in an intramolecular way. Recently, some of us have reported the very first experimental evidence of XB interactions involving astatine.[15] Complexation constants between AtI and a series of

nine Lewis bases were measured in cyclohexane solution. It was shown that these XB interactions were mediated by the astatine atom, in agreement with the differences in the $V_{S,max}$ values determined, through two-component relativistic B3LYP/AVDZ calculations, at the σ-holes of the At and I donor sites in the AtI molecule. However, the quantum calculations also showed that a proportion of the formed XB complexes could be mediated by the iodine atom. This proportion was predicted to be non-negligible for systems with small complexation constants. In this section, we will show quantitatively the influence of spin–orbit coupling on the description of the mixture of XB complexes at equilibrium.

The predicted structures of complexes between AtI and toluene, studied at the 2c-PW6B95/AVTZ level of theory, are displayed in Fig. 2. The calculated distances between AtI and the closest carbon atoms are smaller than the sum of the van der Waals radii of the involved atoms, and the associated bond angles are also close to 180°. These are typical features of XB interactions, although the angle between AtI and the XB acceptor is found to slightly move away from the perfect linearity. Indeed, the nucleophilic sites corresponding to π-electrons of an unsaturated system, here the phenyl ring of toluene, may not coincide with the atoms that form the unsaturated system. One can notice that the XB interaction distances involving astatine are significantly shorter than those involving iodine, despite the larger van der Waals radius of astatine, 2.02 Å,[65] compared with iodine, 1.982 Å. This result is consistent with the predicted greater stability of the IAt···toluene complexes with respect to the AtI···toluene complexes (the free energy gap is at least of 1.3 kcal mol^{-1} at the 2c-PW6B95/AVTZ level of theory). The SOC interaction results in an (may be) unexpected effect since it weakens the AtI···toluene complexes in a greater extent than the IAt···toluene complexes. Indeed, the XB distances involving the iodine atom of AtI are much more increased with SOC (ΔSO > 0.10 Å) than those involving the astatine atom (ΔSO ∼ 0.05 Å). This is a bit surprizing since the relativistic effects are expected to be more pronounced on astatine, this atom being the heavier analogue of iodine.

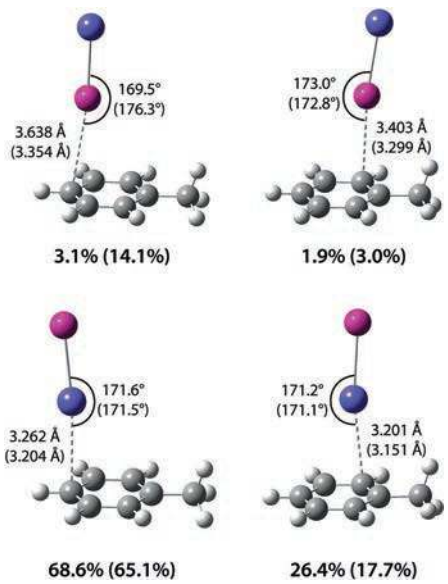

Fig. 2 XB interaction geometries between the AtI and toluene molecules, and corresponding Boltzmann populations, calculated at the 2c-PW6B95/AVTZ level of theory. Values given in parentheses come from spin–orbit free PW6B95/AVTZ calculations. Atom's colour code: purple for At, pink for I, grey for C and white for H.

From an energetic point of view, the stabilities and respective populations of the iodine and astatine-mediated XB complexes are also significantly influenced when SOC is taken into account. Hence, without SOC in the calculations, the AtI···toluene complexes represent a noticeable proportion of the XB complexes, of about 17% (Fig. 2). The picture is significantly modified when SOC is accounted for, since the population of AtI···toluene complexes is divided by three, falling to 5% at the 2c-PW6B95/AVTZ level of theory. In addition, when solvent effects are further introduced by means of a continuum model, the population even decreases to less than 3%, meaning that halogen bonding with iodine becomes a negligible phenomenon.

Clear trends emerge from these results, highlighting the importance of the SOC interaction to delineate, through quantum mechanical calculations, the composition of the XB complexes mixture occurring experimentally. For the system involving AtI and toluene, the astatine site appears as the almost unique XB donor. However, the At *vs.* I competition was considered at a further level in the article of Guo *et al.*[15] AtI can indeed be seen as a I_2 molecule in which one iodine atom has been substituted by the (expected) more potent XB donor, At. The underlying question was tackled through the comparison between (i) the complexation constants (K_{BAtI}) obtained from the reactions between AtI and the nine Lewis bases, and (ii) previously measured complexation constants (K_{BI2})[66] where I_2 was used as the XB donor. The experimental data evidenced that AtI leads in general to stronger XBs, *i.e.* At is revealed to have the greater donating ability. But in the case where toluene is the Lewis base, similar complexation constants have been measured for both AtI and I_2 ($K_{BAtI} = 10^{-0.67\pm0.24}$ and $K_{BI2} = 10^{-0.44}$).[15,66] Hence, for an hypothetical ternary solution of AtI, I_2 and toluene, a true competition between the At donor in AtI and the I donor in I_2 occurs. At the PW6B95/AVTZ level of theory, *i.e.* in the absence of SOC, the K_{BI2} equilibrium constant is calculated to be a factor 1.1 larger than K_{BAtI}. Hence, it is predicted that the complexes stabilized by an I-mediated XB (*i.e.* the I_2···toluene and AtI···toluene complexes) represent 61% of the XB complexes, if AtI and I_2 are present in same amounts. Conversely, the 2c-PW6B95/AVTZ results lead to a K_{BAtI} equilibrium constant 1.1 larger than K_{BI2}, and the astatine complexes then account for 50% of the XB complexes. In addition, when solvent effects are further introduced in the calculations, the proportion of complexes stabilized by an At-mediated XB grows to 58%. Therefore, all performed quantum calculations corroborate the experimental results, *i.e.* the At and I atoms act as competitive XB donors for the considered system. However, an explicit treatment of the SOC effect is found necessary to get a realistic description of the properties of XBs involving At.

Halogen-bond *vs.* hydrogen-bond interactions

In their work, Alkorta *et al.*[25] investigated the XB and hydrogen-bond (HB) complexes of hypohalous acids (from FOH to AtOH)

using the MP2 method and a mix of triple-zeta quality basis sets (MP2/mix). The calculations on I- or At-containing species included the scalar-relativistic effects, through the use of PPs. For a series of three nitrogenated bases (NH_3, HCN and N_2), they established that (i) the HB structures are energetically preferred for FOH, ClOH and BrOH, (ii) the HB and XB interaction energies are similar with IOH, and (iii) the XB complexes are consistently predicted more stable for AtOH. As demonstrated above, the XB complexation energies are significantly affected by the spin–orbit interaction for the heavy astatine atom. It is therefore of interest to study its influence in the context of XB *vs.* HB competition. We have performed some of these calculations at the PW6B95/AVTZ and 2c-PW6B95/AVTZ levels of theory in order to figure out the SOC effect on the complexation geometries and energies. Note that the performance of both PW6B95/AVTZ and MP2/mix calculations are similar, with respect to CCSD(T)/AVQZ interaction energies, as illustrated by the root mean square deviations found, within 1 kcal mol^{-1} (Table S2 in ESI†).

The SOC effects on the HB and the XB complexes are illustrated through the variations of the interatomic distances, gathered in Table 2, and of the complexation energies, reported in Table 3, for the brominated, iodinated and astatinated systems. The spin–orbit interaction does not modify the XB and HB distances for the complexes of hypobromous acid with ammonia as shown by the PW6B95/AVTZ and 2c-PW6B95/AVTZ results. Similarly, the interaction energies (ΔE(HB) and ΔE(XB)) are not significantly affected by the spin–orbit coupling, and the hydrogen-bond donating moiety of BrOH appears to be a stronger Lewis acid than the bromine site, as already emphasized by Alkorta *et al.*[25] With hypoiodous acid, a slight lengthening of the intermolecular distances (*ca.* +0.4%) and a weakening of the interaction energies (*ca.* −2.5%) is observed at the 2c-PW6B95/AVTZ level of theory. If previous MP2/mix calculations predicted similar donating ability for the iodine and hydroxyl groups,[25] the XB complex is found 1.5 kcal mol^{-1} more stable than the HB complex through our DFT calculations. Nevertheless, one must keep in mind that the latter would underestimate hydrogen-bond interactions strength according to the data in Table S2 (ESI†).

The SOC effects are much more substantial for complexes involving hypoastatous acid. A weakening of the interaction energies, ranging from 10% to 20%, is predicted whatever the mode of complexation, halogen-bonded through the astatine atom or hydrogen-bonded through the hydroxyl group. In agreement with the observations of Alkorta *et al.*,[25] the 2c-PW6B95/AVTZ calculations evidence the inversion of the favoured mode of complexation from HB to XB for the astatinated systems. As previously observed, the range of interaction energy follows the order NH_3 > NCH > N_2 for the XB interactions as well as for the HB interactions, and the intermolecular distances increase correspondingly. However, the interaction energies at the 2c-PW6B95/AVTZ level of theory are markedly weaker, from 1.5 to 3.3 kcal mol^{-1}, than the MP2/mix ones. Accordingly, shorter intermolecular distances are systematically observed on MP2/mix geometries, whatever the studied mode of complexation (XB or HB). Furthermore, the relative gap between ΔE(HB) and ΔE(XB) values for a given nitrogen base, is more pronounced at the two-component relativistic level (*ca.* 72%) than that predicted by scalar-relativistic MP2 calculations (*ca.* 43%).

Interestingly, a substantial decrease of the HB complexation energies of AtOH is predicted (from 17% to 19%, Table 3) when the spin–orbit interaction is taken into account. This weakening is even larger than that observed for XB interactions involving directly the astatine atom (from 11% to 16%). Both $V_{S,max}$ and $\omega^{+}_{S,max}$ descriptors have been calculated for AtOH at the PW6B95/AVTZ and 2c-PW6B95/AVTZ levels of theory. In agreement with the ΔE(HB) and ΔE(XB) evolutions, the SOC leads to a more significant reduction of the electrostatic potential and local electrophilicity values in the vicinity of the HB interacting site (−12% and −18%, respectively) in comparison with the XB interacting site (−3% and −14%, respectively). Since the hydrogen atom (i) is not directly bounded to astatine, and (ii) is the lightest element, it is of particular interest to highlight that the astatine relativistic effects are propagated on the hydrogen chemical properties with higher magnitude than on its own chemical properties. However, it is

Table 2 Optimized interatomic distances (in Å) of the HB and XB complexes between XOH hypohalous acids and nitrogenated bases

	MP2/mix[a]		PW6B95/AVTZ		2c-PW6B95/AVTZ	
	$d_{H\cdots N}$	$d_{X\cdots N}$	$d_{H\cdots N}$	$d_{X\cdots N}$	$d_{H\cdots N}$[b]	$d_{X\cdots N}$[b]
BrOH–NH_3	1.784	2.612	1.815	2.550	1.816 (+0.1%)	2.550 (+0.0%)
IOH–NH_3	1.794	2.663	1.839	2.650	1.848 (+0.5%)	2.659 (+0.3%)
AtOH–NH_3	1.826	2.678	1.871	2.684	1.925 (+2.9%)	2.753 (+2.6%)
AtOH–NCH	1.965	2.749	2.039	2.749	2.100 (+3.0%)	2.854 (+3.8%)
AtOH–N_2	2.217	2.992	2.392	3.029	2.469 (+3.2%)	3.141 (+3.7%)

[a] Mixed basis sets with def2-TZVPP for the halogen atoms and 6-311++G(2d,2p) for the remaining atoms.[25] [b] The relative lengthening observed upon SOC is given in parenthesis.

Table 3 HB and XB interaction energies (in kcal mol^{-1}) between XOH hypohalous acids and nitrogenated bases

	MP2/mix[a]		PW6B95/AVTZ		2c-PW6B95/AVTZ	
	ΔE(HB)	ΔE(XB)	ΔE^{CP}(HB)	ΔE^{CP}(XB)	ΔE^{CP}(HB)[b]	ΔE^{CP}(XB)[b]
BrOH–NH_3	−11.02	−7.43	−9.54	−8.09	−9.50 (−0.4%)	−8.07 (−0.2%)
IOH–NH_3	−10.77	−10.85	−8.96	−10.50	−8.73 (−2.5%)	−10.25 (−2.4%)
AtOH–NH_3	−10.02	−13.77	−8.10	−12.82	−6.73 (−16.9%)	−11.04 (−13.9%)
AtOH–NCH	−6.30	−8.83	−4.49	−7.10	−3.70 (−17.6%)	−6.31 (−11.1%)
AtOH–N_2	−2.49	−3.75	−1.24	−2.17	−1.00 (−19.2%)	−1.82 (−16.5%)

[a] Mixed basis sets with def2-TZVPP for the halogen atoms and 6-311++G(2d,2p) for the remaining atoms.[25] [b] The relative decrease observed upon SOC is given in parenthesis.

established that astatine electronegativity is strongly decreased upon SOC (about 10%).[32,35] This should imply in AtOH species a significant shift of the electronic charge toward the more electronegative oxygen atom, and for the more distant hydrogen atom, a potential attenuation of its HB donating ability.

Conclusions

The importance of spin–orbit coupling on astatine-mediated halogen bonds is examined by quantum chemistry using compounds previously investigated through more conventional theoretical methods (*i.e.* by spin–orbit free relativistic calculations). The magnitude of SOC is emphasized in the astatinated systems, leading to a sizeable decrease of the halogen-bond donating ability. The effect is prominent enough for inverting the expected trend in the $X_2\cdots NH_3$ series.[28] Despite the larger astatine polarizability over iodine, I_2 leads to a stronger halogen-bond interaction than At_2 when SOC is considered. This outcome can be foreseen from the analysis, in bare XB donors, of appropriate descriptors dedicated to probe electrostatic and charge-transfer interactions. The competition between the I and At atoms as XB donors was also investigated at an intramolecular level in astatine monoiodide, AtI. Astatine remains the preferred interaction site whatever the level of theory. However, the At-mediated XB complexes are in minority (39%) in a hypothetical AtI, I_2 and toluene mixture, through scalar relativistic calculations, while they are predominant in solution (58%) when SOC is taken into account. Hence, an explicit treatment of the relativistic spin–orbit interaction is found necessary to get a realistic description of the mixture composition. Finally, the propensity of hypoastatous acid, AtOH, to behave as halogen- and/or hydrogen-bond donor was studied. XB interaction energies are found to be reduced by SOC up to 17%, but the XB donating ability of the At atom is always greater than the HB donating ability of the OH moiety. Calculated values of the maxima of the local electrophilicity ($\omega^{+}_{S,max}$) and of the electrostatic potential ($V_{S,max}$) at the molecular surface of AtOH corroborate this result.

In addition, our results show that, although the SOC effects can deeply affect the properties of astatine, this influence can be even more pronounced on neighbouring atoms. Thus, the study of XB complexes formed with AtI has shown that the iodine-mediated halogen bonds are more weakened upon SOC than the astatine-mediated ones. Similarly, the ability of AtOH to form hydrogen bonds appears, proportionally, the most affected by the spin–orbit coupling despite the At heavy element is not directly involved in the interaction. It was thus demonstrated that a strong transfer of spin-dependent relativistic effects (initiated by astatine core-electrons) occurs through space towards the peripheral hydrogen atom. The spatial dimension of relativistic effects has previously been widely discussed at the atomic level.[67–69] According to our results, an electronic vector, able to transmit the SOC effects beyond an atomic horizon, is playing a key role on the interacting ability of chemical functions in the vicinity of astatine. We anticipate that the driving force of this phenomenon is the electronegativity. Such hypothesis is currently under active investigations in our group.

Conflicts of interest

There are no conflicts to declare.

Acknowledgements

This work has been supported in part by grants from the French National Agency for Research called ''Investissements d'Avenir'' (ANR-11-EQPX-0004, ANR-11-LABX-0018). It was carried out using HPC resources from GENCI-CINES/IDRIS (grant A0020805117) and from CCIPL (''Centre de Calcul Intensif des Pays de la Loire'').

References

1 D. S. Wilbur, *Nat. Chem.*, 2013, **5**, 246.
2 M. R. Zalutsky and M. Pruszynski, *Curr. Radiopharm.*, 2011, **4**, 177–185.
3 D. S. Wilbur, *Curr. Radiopharm.*, 2008, **1**, 144–176.
4 G. Vaidyanathan and M. R. Zalutsky, *Curr. Radiopharm.*, 2011, **4**, 283–294.
5 F. Guérard, J.-F. Gestin and M. W. Brechbiel, *Cancer Biother. Radiopharm.*, 2012, **28**, 1–20.
6 J. G. Hamilton and M. H. Soley, *Proc. Natl. Acad. Sci. U. S. A.*, 1940, **26**, 483–489.
7 J. G. Hamilton, C. W. Asling, W. M. Garrison and K. G. Scott, *Univ. Calif. Publ. Pharmacol.*, 1953, **2**, 283–312.
8 S. W. Hadley, D. S. Wilbur, M. A. Gray and R. W. Atcher, *Bioconjugate Chem.*, 1991, **2**, 171–179.
9 G. L. Johnson, R. F. Leininger and E. Segrè, *J. Chem. Phys.*, 1949, **17**, 1–10.
10 V. D. Nefedov, Y. V. Norseev, K. Savlevich, E. N. Sinotova, M. A. Toropova and V. A. Khalkin, *Dokl. Akad. Nauk SSSR*, 1962, 866.
11 E. H. Appelman, E. N. Sloth and M. H. Studier, *Inorg. Chem.*, 1966, **5**, 766–769.
12 A. Sabatié-Gogova, J. Champion, S. Huclier, N. Michel, F. Pottier, N. Galland, Z. Asfari, M. Chérel and G. Montavon, *Anal. Chim. Acta*, 2012, **721**, 182–188.
13 T. Fleig and A. J. Sadlej, *Phys. Rev. A: At., Mol., Opt. Phys.*, 2002, **65**, 032506.
14 G. Cavallo, P. Metrangolo, R. Milani, T. Pilati, A. Priimagi, G. Resnati and G. Terraneo, *Chem. Rev.*, 2016, **116**, 2478–2601.
15 N. Guo, R. Maurice, D. Teze, J. Graton, J. Champion, G. Montavon and N. Galland, *Nat. Chem.*, 2018, DOI: 10.1038/s41557-018-0011-1.
16 J. Champion, C. Alliot, E. Renault, B. M. Mokili, M. Cherel, N. Galland and G. Montavon, *J. Phys. Chem. A*, 2010, **114**, 576–582.
17 J. Champion, M. Seydou, A. Sabatié-Gogova, E. Renault, G. Montavon and N. Galland, *Phys. Chem. Chem. Phys.*, 2011, **13**, 14984–14992.

18 J. Champion, A. Sabatié-Gogova, F. Bassal, T. Ayed, C. Alliot, N. Galland and G. Montavon, *J. Phys. Chem. A*, 2013, **117**, 1983–1990.
19 T. Ayed, M. Seydou, F. Réal, G. Montavon and N. Galland, *J. Phys. Chem. B*, 2013, **117**, 5206–5211.
20 T. Ayed, F. Réal, G. Montavon and N. Galland, *J. Phys. Chem. B*, 2013, **117**, 10589–10595.
21 T. Ayed, J. Pilmé, D. Tézé, F. Bassal, J. Barbet, M. Chérel, J. Champion, R. Maurice, G. Montavon and N. Galland, *Eur. J. Med. Chem.*, 2016, **116**, 156–164.
22 N. Guo, D.-C. Sergentu, D. Teze, J. Champion, G. Montavon, N. Galland and R. Maurice, *Angew. Chem., Int. Ed.*, 2016, **55**, 15369–15372.
23 D.-C. Sergentu, D. Teze, A. Sabatié-Gogova, C. Alliot, N. Guo, F. Bassal, I. D. Silva, D. Deniaud, R. Maurice, J. Champion, N. Galland and G. Montavon, *Chem. – Eur. J.*, 2016, **22**, 2964–2971.
24 D. Teze, D.-C. Sergentu, V. Kalichuk, J. Barbet, D. Deniaud, N. Galland, R. Maurice and G. Montavon, *Sci. Rep.*, 2017, **7**, 2579.
25 I. Alkorta, F. Blanco, M. Solimannejad and J. Elguero, *J. Phys. Chem. A*, 2008, **112**, 10856–10863.
26 S. W. L. Hogan and T. van Mourik, *J. Comput. Chem.*, 2016, **37**, 763–770.
27 G. Huan, T. Xu, R. Momen, L. Wang, Y. Ping, S. R. Kirk, S. Jenkins and T. van Mourik, *Chem. Phys. Lett.*, 2016, **662**, 67–72.
28 J. G. Hill and X. Hu, *Chem. – Eur. J.*, 2013, **19**, 3620–3628.
29 P. Norman, B. Schimmelpfennig, K. Ruud, H. J. A. Jensen and H. Ågren, *J. Chem. Phys.*, 2002, **116**, 6914–6923.
30 J. Pilmé, E. Renault, T. Ayed, G. Montavon and N. Galland, *J. Chem. Theory Comput.*, 2012, **8**, 2985–2990.
31 A. Hermann, R. Hoffmann and N. W. Ashcroft, *Phys. Rev. Lett.*, 2013, **111**, 116404.
32 J. Pilmé, E. Renault, F. Bassal, M. Amaouch, G. Montavon and N. Galland, *J. Chem. Theory Comput.*, 2014, **10**, 4830–4841.
33 A. Severo Pereira Gomes, F. Réal, R. Cimiraglia, V. Vallet, C. Angeli and N. Galland, *Phys. Chem. Chem. Phys.*, 2014, **16**, 9238.
34 R. Maurice, F. Réal, A. S. P. Gomes, V. Vallet, G. Montavon and N. Galland, *J. Chem. Phys.*, 2015, **142**, 094305.
35 D.-C. Sergentu, G. David, G. Montavon, R. Maurice and N. Galland, *J. Comput. Chem.*, 2016, **37**, 1345–1354.
36 T. Saue, *ChemPhysChem*, 2011, **12**, 3077–3094.
37 J. Autschbach, *J. Chem. Phys.*, 2012, **136**, 150902.
38 M. Dolg and X. Cao, *Chem. Rev.*, 2012, **112**, 403–480.
39 T. Fleig, *Chem. Phys.*, 2012, **395**, 2–15.
40 Y. J. Choi and Y. S. Lee, *J. Chem. Phys.*, 2003, **119**, 2014–2019.
41 D.-D. Yang and F. Wang, *Phys. Chem. Chem. Phys.*, 2012, **14**, 15816.
42 H. Kim, Y. J. Choi and Y. S. Lee, *J. Phys. Chem. B*, 2008, **112**, 16021–16029.
43 T. P. Straatsma, E. Apra, T. L. Windus, E. J. Bylaska, W. A. de Jong, S. Hirata, M. Valiev, M. Hackler, L. Pollack and R. J. Harrison, *NWChem, A Computational Chemistry Package for Parallel Computers*, Pacific Northwest National Laboratory, Richland, Washington, 2008.
44 Y. Zhao and D. G. Truhlar, *J. Phys. Chem. A*, 2005, **109**, 5656–5667.
45 K. A. Peterson, D. Figgen, E. Goll, H. Stoll and M. Dolg, *J. Chem. Phys.*, 2003, **119**, 11113–11123.
46 K. A. Peterson, B. C. Shepler, D. Figgen and H. Stoll, *J. Phys. Chem. A*, 2006, **110**, 13877–13883.
47 M. K. Armbruster, W. Klopper and F. Weigend, *Phys. Chem. Chem. Phys.*, 2006, **8**, 4862.
48 T. H. Dunning, *J. Chem. Phys.*, 1989, **90**, 1007–1023.
49 R. A. Kendall, T. H. Dunning and R. J. Harrison, *J. Chem. Phys.*, 1992, **96**, 6796–6806.
50 D. E. Woon and T. H. Dunning, *J. Chem. Phys.*, 1993, **98**, 1358–1371.
51 S. F. Boys and F. Bernardi, *Mol. Phys.*, 1970, **19**, 553–556.
52 M. Cossi, N. Rega, G. Scalmani and V. Barone, *J. Comput. Chem.*, 2003, **24**, 669–681.
53 M. J. Frisch, G. W. Trucks, H. B. Schlegel, G. E. Scuseria, M. A. Robb, J. R. Cheeseman, G. Scalmani, V. Barone, G. A. Petersson, H. Nakatsuji, X. Li, M. Caricato, A. V. Marenich, J. Bloino, B. G. Janesko, R. Gomperts, B. Mennucci, H. P. Hratchian, J. V. Ortiz, A. F. Izmaylov, J. L. Sonnenberg, D. Williams-Young, F. Ding, F. Lipparini, F. Egidi, J. Goings, B. Peng, A. Petrone, T. Henderson, D. Ranasinghe, V. G. Zakrzewski, J. Gao, N. Rega, G. Zheng, W. Liang, M. Hada, M. Ehara, K. Toyota, R. Fukuda, J. Hasegawa, M. Ishida, T. Nakajima, Y. Honda, O. Kitao, H. Nakai, T. Vreven, K. Throssell, J. A. Montgomery Jr., J. E. Peralta, F. Ogliaro, M. J. Bearpark, J. J. Heyd, E. N. Brothers, K. N. Kudin, V. N. Staroverov, T. A. Keith, R. Kobayashi, J. Normand, K. Raghavachari, A. P. Rendell, J. C. Burant, S. S. Iyengar, J. Tomasi, M. Cossi, J. M. Millam, M. Klene, C. Adamo, R. Cammi, J. W. Ochterski, R. L. Martin, K. Morokuma, O. Farkas, J. B. Foresman and D. J. Fox, *Gaussian 16*, Wallingford, CT, 2016.
54 V. Barone, M. Cossi and J. Tomasi, *J. Chem. Phys.*, 1997, **107**, 3210–3221.
55 TURBOMOLE V6.6 2014, a development of University of Karlsruhe and Forschungszentrum Karlsruhe GmbH, 1989–2007, TURBOMOLE GmbH, since 2007; available from http://www.turbomole.com.
56 L. Visscher and K. G. Dyall, *J. Chem. Phys.*, 1996, **104**, 9040–9046.
57 T. Saue, K. Faegri and O. Gropen, *Chem. Phys. Lett.*, 1996, **263**, 360–366.
58 Y.-K. Han, C. Bae, S.-K. Son and Y. S. Lee, *J. Chem. Phys.*, 2000, **112**, 2684–2691.
59 M. Amaouch, E. Renault, G. Montavon, N. Galland and J. Pilmé, *Applications of Topological Methods in Molecular Chemistry*, Springer, Cham, 2016, pp. 553–582.
60 T. Clark, M. Hennemann, J. S. Murray and P. Politzer, *J. Mol. Model.*, 2007, **13**, 291–296.
61 M. H. Kolář and P. Hobza, *Chem. Rev.*, 2016, **116**, 5155–5187.
62 C. Wang, D. Danovich, Y. Mo and S. Shaik, *J. Chem. Theory Comput.*, 2014, **10**, 3726–3737.
63 F. Guégan, P. Mignon, V. Tognetti, L. Joubert and C. Morell, *Phys. Chem. Chem. Phys.*, 2014, **16**, 15558–15569.

64 P. K. Chattaraj, U. Sarkar and D. R. Roy, *Chem. Rev.*, 2006, **106**, 2065–2091.
65 M. Mantina, A. C. Chamberlin, R. Valero, C. J. Cramer and D. G. Truhlar, *J. Phys. Chem. A*, 2009, **113**, 5806–5812.
66 C. Laurence, J. Graton, M. Berthelot and M. J. El Ghomari, *Chem. – Eur. J.*, 2011, **17**, 10431–10444.
67 S. J. Rose, I. P. Grant and N. C. Pyper, *J. Phys. B: At. Mol. Phys.*, 1978, **11**, 1171.
68 M. Barysz and Y. Ishikawa, *Relativistic Methods for Chemists*, Springer, 2010.
69 K. G. Dyall and K. Fægri Jr, *Introduction to Relativistic Quantum Chemistry*, Oxford University Press, Oxford, New York, 2007.

Quantum calculations of At-mediated halogen bonds: on the influence of relativistic effects

N. Galland,[a,*] G. Montavon,[b] J.-Y. Le Questel,[a] J. Graton[a,*]

[a] Laboratoire CEISAM, UMR CNRS 6230, Université de Nantes, 2 rue de la Houssinière, BP 92208, Nantes Cedex 3, 44322, France. Nicolas.Galland@univ-nantes.fr, Jerome.Graton@univ-nantes.fr
[b] Laboratoire SUBATECH, UMR CNRS 6457, IN2P3/EMN Nantes/Université de Nantes, 4 Rue Alfred Kastler, BP 20722, Nantes Cedex 3, 44307, France.

New Journal of Chemistry

Table S1. Counterpoise corrected intermolecular and intrahalogen bond lengths, variation of the intrahalogen bond length as a result of $X_2\cdots NH_3$ formation, and interaction energy.

	$d_{X\ldots N}$ (Å)	d_{X-X} (Å)	Δd_{X-X} (Å)	ΔE^{CP} (kcal mol^{-1})
I–I···NH$_3$				
CP-CCSD(T)-F12b/VTZ-F12 [28]	2.767	2.720	+0.041	-7.90 [a]
CP-PW6B95/AVTZ	2.723	2.725	+0.056	-8.22
At–At···NH$_3$				
CP-CCSD(T)-F12b/VTZ-F12 [28]	2.782	2.900	+0.042	-9.54 [a]
CP-PW6B95/AVTZ	2.756	2.899	+0.054	-9.69

[a] Extrapolation to the complete basis set limit.

Table S2. HB and XB interaction energies (in kcal mol^{-1}) between XOH hypohalous acids and nitrogenated bases.

	CCSD(T)/AVQZ//PW6B95/AVTZ		MP2/mix [a]		PW6B95/AVTZ	
	ΔE(HB)	**ΔE(XB)**	**ΔE(HB)** [b]	**ΔE(XB)** [b]	**ΔE(HB)** [b]	**ΔE(XB)** [b]
FOH-NH$_3$	-11.11		-11.02 (+0.09)		-10.74 (+0.37)	
ClOH-NH$_3$	-11.09	-4.24	-11.24 (-0.15)	-4.44 (-0.20)	-10.34 (+0.75)	-4.13 (+0.10)
BrOH-NH$_3$	-10.59	-7.68	-11.02 (-0.43)	-7.43 (+0.25)	-9.65 (+0.93)	-8.17 (-0.49)
IOH-NH$_3$	-10.14	-10.29	-10.77 (-0.64)	-10.85 (-0.56)	-9.07 (+1.07)	-10.60 (-0.31)
AtOH-NH$_3$	-9.32	-12.78	-10.02 (-0.70)	-13.77 (-1.00)	-8.21 (+1.11)	-12.95 (-0.18)
AtOH-NCH	-5.65	-7.50	-6.30 (-0.65)	-8.83 (-1.33)	-4.64 (+1.02)	-7.29 (+0.21)
AtOH-N$_2$	-1.99	-2.68	-2.49 (-0.50)	-3.75 (-1.07)	-1.34 (+0.65)	-2.32 (+0.36)
		RMSD	0.51	0.85	0.88	0.30

[a] Mixed basis sets with def2-TZVPP for the halogen atoms and 6-311++G(2d,2p) for the remaining atoms.[25] [b] The deviation with respect to the CCSD(T)/AVQZ//PW6B95/AVTZ results is given in parenthesis.

Structures S1. Cartesian coordinates (in Å) at the 2*c*-PW6B95/AVTZ level of theory for the interaction structures between At_2 and ammonia.

H	0.66670006	0.66670006	4.39479982
H	0.24402916	-0.91072921	4.39479982
H	-0.91072921	0.24402916	4.39479982
At	0.00000000	0.00000000	-1.82822806
At	0.00000000	0.00000000	1.18875916
N	0.00000000	0.00000000	4.03799525

Structures S2. Cartesian coordinates (in Å) and relative free energies (ΔG^0_{298}) at the 2*c*-PW6B95/AVTZ level of theory for the interaction structures between the AtI and toluene molecules.

At-mediated interaction: ΔG^0_{298} = 0 kcal mol^{-1}

C	-1.1034051527	3.8067469902 -0.0097256112
C	-0.4592531774	3.6706332154 1.2159578396
C	0.8272316591	3.1759974291 1.2950920678
C	1.5044003109	2.8078677175 0.1406587722
C	0.8742888007	2.9420095436 -1.0887170399
C	-0.4175805911	3.438151249 -1.1572661889
H	-0.9764982008	3.9567572876 2.1187352651
H	1.3084580767	3.0798788763 2.2546651206
H	2.5180685113	2.4455546624 0.1958076135
H	1.3951744768	2.673989205 -1.9937622445
H	-0.8983279572	3.5406244448 -2.1176251126
C	-2.5099370701	4.3128416443 -0.0809429265
H	-3.2171790394	3.5143170656 0.1345299328
H	-2.6820272926	5.1022662839 0.6443408435
H	-2.7412902021	4.698615161 -1.0682235829
At	0.3670422942	-0.2383183482 -0.1142505114
I	-0.3897049763	-2.9914797474 -0.0039150572

I-mediated interaction: ΔG^0_{298} = 1.8 kcal mol^{-1}

C	0.0004934664	0.0006504972 -0.0001724774
C	0.0004947446	-0.0000477107 1.3889607389
C	1.2235441768	0.000400713 2.0454068202
C	2.4130418889	-0.0066797051 1.3377116944
C	2.3983711518	-0.0128151169 -0.047540364
C	1.1847220853	-0.0074711428 -0.7138985329
C	-1.2841808889	-0.0321521563 2.1573090222
I	2.1807218941	-3.5725943541 0.6708880688
At	2.0641864494	-6.4099897766 0.7174358632
H	1.2449979074	0.0047871873 3.1244073036
H	3.3519799227	-0.0051108422 1.8675326308
H	3.323111911	-0.0165379897 -0.6009048264
H	1.1611554749	-0.0096032707 -1.791641971
H	-0.940784461	0.0053962637 -0.5282353541
H	-1.5970416087	-1.05814601 2.3421587726
H	-1.1800635474	0.4552783731 3.1216329537
H	-2.0835496415	0.458826534 1.6110899916

At-mediated interaction: ΔG^0_{298} = 0.6 kcal mol^{-1}

C	-1.0141996592	-3.2449238649 -0.1621352992
C	-0.2092253384	-2.9768961031 0.94462875
C	1.1740206588	-3.0431217226 0.8544156319
C	1.776871148	-3.3865849913 -0.3445339281
C	0.9876337509	-3.6640009209 -1.4443138397
C	-0.3928487868	-3.591875197 -1.3516897909
H	-0.6716163698	-2.7376285237 1.8904687986
H	1.7765704404	-2.8385307764 1.7246358181
H	2.8504316289	-3.4390495343 -0.4163887265
H	1.4458203268	-3.9356072052 -2.3814309723
H	-0.9977088828	-3.8068757374 -2.218782711
C	-2.5030730234	-3.1375744718 -0.0635760413
H	-2.8766449848	-3.6352300392 0.8267882188
H	-2.8091684439	-2.0945033564 -0.0037895052
H	-2.9877115603	-3.5765099926 -0.9288878221
At	0.1144694943	0.1504979108 0.3449946304
I	-0.0219949585	2.973161656 -0.0804385714

I-mediated interaction: ΔG^0_{298} = 2.1 kcal mol^{-1}

C	0.0049001386	-0.0115245721 -0.0047706496
C	0.0081669526	0.0109334716 1.3822297495
C	1.2375537134	0.0118940494 2.0354305745
C	2.4244919295	-0.001668651 1.3222777157
C	2.4038194082	-0.0205109344 -0.0612182835
C	1.1889439784	-0.0275930926 -0.7217954821
C	-1.2693172885	0.0608109181 2.1604559775
I	1.1247181253	3.4099690376 2.1818202617
At	0.8541843226	6.2099249296 2.6034673508
H	1.2631780427	0.0158364444 3.1146148036
H	3.3648238796	0.0006847269 1.8494569489
H	3.3262057926	-0.031046592 -0.6182038843
H	1.1609529637	-0.0445169428 -1.7994139303
H	-0.9378481387	-0.0150620284 -0.5298628806
H	-1.2453494	-0.6236187317 3.0036663024
H	-1.4361867938	1.0603281453 2.5582879431
H	-2.1201800253	-0.1948960984 1.5377298977

Structures S3. Cartesian coordinates (in Å) at the 2*c*-PW6B95/AVTZ level of theory for the interaction structures between the AtOH and nitrogenated bases.

AtOH-NH_3 HB complex

N	3.458160	-0.399860	0.000000
H	3.281238	-1.392683	0.000004
H	4.017295	-0.191856	0.813182
H	4.017294	-0.191863	-0.813184
H	1.876197	0.696518	-0.000001
At	-0.542317	-0.074122	0.000000
O	1.087223	1.272405	0.000000

AtOH-NH_3 XB complex

N	-0.037415	-2.666754	0.000000
H	-0.986334	-3.007871	0.000000
H	0.425580	-3.036955	0.815588
H	0.425580	-3.036955	-0.815588
H	0.854932	2.534914	0.000000
At	0.000000	0.085728	0.000000
O	-0.057232	2.240911	0.000000

AtOH-NCH HB complex

N	-0.497867	3.380823	0.000000
C	-1.036817	4.385802	0.000000
H	-1.538656	5.322516	0.000000
H	0.734820	1.680941	0.000000
At	-0.000000	-0.755905	0.000000
O	1.313726	0.908482	0.000000

AtOH-NCH XB complex

N	-0.008336	-2.5816	0.000000
C	-0.020096	-3.721516	0.000000
H	-0.031369	-4.784451	0.000000
H	0.833266	2.710993	0.000000
At	0.000000	0.272652	0.000000
O	-0.077871	2.412288	0.000000

AtOH-N_2 HB complex

N	0.588818	3.321603	0.000000
N	1.395890	4.049038	0.000000
H	-1.160042	1.578147	0.000000
At	0.000000	-0.693309	0.000000
O	-1.591614	0.719829	0.000000

AtOH-N_2 XB complex

N	-0.015508	-2.843791	0.000000
N	-0.017502	-3.930323	0.000000
H	0.837739	2.721145	0.000000
At	0.000000	0.297437	0.000000
O	-0.075834	2.426944	0.000000